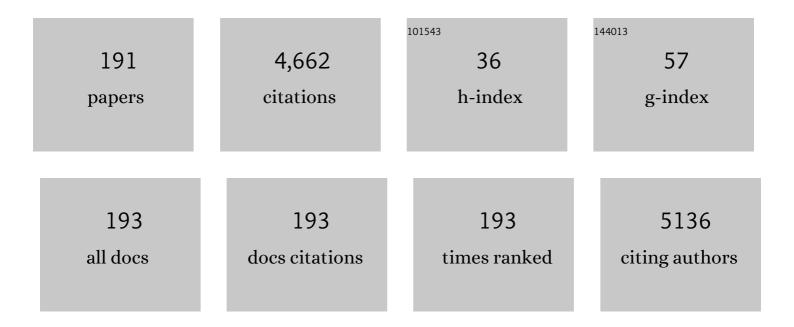
## Sumantra Kumar Pradhan

List of Publications by Year in descending order

Source: https://exaly.com/author-pdf/2765823/publications.pdf Version: 2024-02-01



#	Article	IF	CITATIONS
1	Improved thermoelectric performance of nanostructured Bi2Te3 fabricated by solvent-free mechanical alloying. Materials Chemistry and Physics, 2022, 279, 125736.	4.0	6
2	Nanoplate like heterostructured BiOBr/BiBr/FeBr2 nanocomposites with enhanced photocatalytic activity for wastewater treatment by removing organic dyes: Interfacial consecutive dual Z scheme electron transfer. Journal of Environmental Chemical Engineering, 2022, 10, 107240.	6.7	12
3	Microstructure and morphology related electrical characterization and dielectric relaxation studies of nanocrystalline Sb2Te3 synthesized by mechanical alloying. Materials Science and Engineering B: Solid-State Materials for Advanced Technology, 2022, 278, 115647.	3.5	5
4	Enhanced hydrogen evolution rate using Mg-Cu Galvanic Coupling electrodes and seawater electrolyte. Materials Letters, 2022, 315, 131946.	2.6	3
5	Study of microstructural and electrical properties of silver substituted hydroxyapatite for drug delivery applications. Materials Today Communications, 2022, 31, 103360.	1.9	7
6	A novel strategy for the enhancement of the antibacterial activity of ciprofloxacin by conjugating it with a biocompatible nanocomposite. AIP Conference Proceedings, 2022, , .	0.4	0
7	Microstructure, optical and electrical characterizations of Bi-incorporated Sb2Te3 thermoelectric compound synthesized by mechanical alloying: A comparative study with undoped Sb2Te3. Materials Today: Proceedings, 2022, , .	1.8	3
8	Ultrastable Asymmetric Supercapacitor Device with Chemically Derived and Mechanically Activated NiCo <sub>2</sub> O <sub>4</sub> . Energy & Fuels, 2022, 36, 7878-7889.	5.1	8
9	A comparative study on the antibacterial activities of TiO2-Ag nanocomposites with the different molar percentages of Ag. Materials Today: Proceedings, 2022, 66, 3283-3286.	1.8	0
10	Enhanced antibacterial activity of a novel protein-arginine deiminase type-4 (PADI4) inhibitor after conjugation with a biocompatible nanocarrier. Journal of Drug Delivery Science and Technology, 2022, 74, 103549.	3.0	1
11	On the grain boundary character evolution in non equiatomic high entropy alloy during hot rolling induced dynamic recrystallization. Journal of Alloys and Compounds, 2022, 922, 166126.	5.5	7
12	Synthesis of drug conjugated magnetic nanocomposite with enhanced hypoglycemic effects. Materials Science and Engineering C, 2021, 120, 111697.	7.3	11
13	Enhanced electrochemical properties of Co3O4 with morphological hierarchy for energy storage application: A comparative study with different electrolytes. Journal of Physics and Chemistry of Solids, 2021, 148, 109733.	4.0	21
14	Grain size mediated electrical and thermoelectric performances of mechanically alloyed Sb2Te3 nanoparticles. Journal of Alloys and Compounds, 2021, 858, 157732.	5.5	13
15	Comprehending the role of individual microstructural features on electrochemical response and passive film behaviour in type 304 austenitic stainless steel. Corrosion Science, 2021, 180, 109187.	6.6	47
16	Spectacular photocatalytic activity of mechanosynthesized heterostructured Bi-Fe-O nanocomposites in wastewater treatment containing colored and colorless pollutants. Journal of Molecular Liquids, 2021, 326, 115317.	4.9	6
17	Evolution of geometrically necessary dislocation at the γ-γ′ interface and its effect on tensile deformation behaviour of disk super alloy. Materials Science & Engineering A: Structural Materials: Properties, Microstructure and Processing, 2021, 807, 140855.	5.6	7
18	Synthesis and characterization of a novel drug conjugated copper-silver- titanium oxide nanocomposite with enhanced antibacterial activity. Journal of Drug Delivery Science and Technology, 2021, 62, 102384.	3.0	11

#	Article	IF	CITATIONS
19	Superior photocatalytic performance of mechanosynthesized Bi2O3–Bi2WO6 nanocomposite in wastewater treatment. Solid State Sciences, 2021, 115, 106587.	3.2	15
20	Strain-induced microstructural evolution and its implication on high-temperature hot corrosion (HTHC) phenomena in Alloy 617. Materials Characterization, 2021, 178, 111272.	4.4	3
21	Effect of stacking faults on structural, morphological, and electrical properties of hydroxyapatite polycrystals. Materials Letters, 2021, 298, 130001.	2.6	4
22	Structure, photoluminescence, and electrical transport properties of pure and Eu2O3 activated Zn2SnO4 host matrix. Solid State Sciences, 2021, 121, 106744.	3.2	4
23	Synthesis and characterization of a novel nanocarrier for biocompatible targeting of an antibacterial therapeutic agent with enhanced activity. Journal of Drug Delivery Science and Technology, 2021, 66, 102821.	3.0	3
24	MWCNT incorporated wool-ball-like CuO@NiO hybrid nanostructures for high-performance energy storage device. Journal of Alloys and Compounds, 2021, 886, 161313.	5.5	10
25	Composition related structural transition between mechanosynthesized CsPbBr3 and CsPb2Br5 perovskites andÂtheirÂoptical properties. Journal of Alloys and Compounds, 2020, 816, 152612.	5.5	28
26	Enhanced antifungal activity of fluconazole conjugated with Cu-Ag-ZnO nanocomposite. Materials Science and Engineering C, 2020, 106, 110160.	7.3	37
27	Advanced asymmetric supercapacitor with NiCo2O4 nanoparticles and nanowires electrodes: A comparative morphological hierarchy. Journal of Alloys and Compounds, 2020, 821, 153503.	5.5	28
28	Optimized enhanced photodegradation activity of sintered molybdenum oxide: A morphological hierarchy in wastewater treatment. Materials Research Bulletin, 2020, 124, 110760.	5.2	2
29	A potential insight into the serration behaviour of Σ3n (nâ‰ <b>8</b> ) boundaries in Alloy 617. Materials Chemistry and Physics, 2020, 248, 122919.	4.0	14
30	â€~Hall-Petch' type of relationship between the extent of intergranular corrosion and grain size in a Ni-based superalloy. Corrosion Science, 2020, 175, 108868.	6.6	17
31	Dielectric response of ZrO2–CeO2 nanocrystalline solid solution above room temperature. Physica B: Condensed Matter, 2020, 583, 412000.	2.7	1
32	Enhanced photocatalysis performance of mechano-synthesized V2O5–TiO2 nanocomposite for wastewater treatment: Correlation of structure with photocatalytic performance. Materials Chemistry and Physics, 2020, 248, 122947.	4.0	25
33	Enhanced photocatalytic and antibacterial activities of mechanosynthesized TiO2–Ag nanocomposite in wastewater treatment. Journal of Molecular Structure, 2020, 1211, 128076.	3.6	32
34	Morphological effects on the photocatalytic properties of SnO2 nanostructures. Journal of Alloys and Compounds, 2019, 810, 151718.	5.5	57
35	Influence of the individual microstructural features on pitting corrosion in type 304 austenitic stainless steel. Corrosion Science, 2019, 158, 108091.	6.6	67
36	Ultra-Low-Temperature CO Oxidation Activity of Octahedral Site Cobalt Species in Co <sub>3</sub> O <sub>4</sub> Based Catalysts: Unravelling the Origin of the Unique Catalytic Property. Journal of Physical Chemistry C, 2019, 123, 19557-19571.	3.1	41

#	Article	IF	CITATIONS
37	Effect of sintering on the structure, microstructure and electrical properties of mechanosynthesized Y2O3 and Dy2O3 alloyed ceria nanoparticles: A comparative study. Materials Research Bulletin, 2019, 120, 110582.	5.2	1
38	Enhanced photocatalytic performance of V <sub>2</sub> O <sub>5</sub> –TiO <sub>2</sub> nanocomposites synthesized by mechanical alloying with morphological hierarchy. New Journal of Chemistry, 2019, 43, 2804-2816.	2.8	29
39	Microstructure characterization of biocompatible heterojunction hydrogen titanate-Ag2O nanocomposites for superior visible light photocatalysis and antibacterial activity. Materials Science and Engineering C, 2019, 99, 374-386.	7.3	14
40	Effect of lattice distortion in optical properties of CeO2 nanocrystals on Mn substitution by mechanical alloying. Journal of Alloys and Compounds, 2019, 786, 215-224.	5.5	16
41	Microstructure correlated ferromagnetism in manganese stabilized zirconia nanoparticles. Journal of Alloys and Compounds, 2019, 793, 220-231.	5.5	3
42	Structural interpretation, microstructure characterization, mechanical properties, and cytocompatibility study of pure and doped carbonated nanocrystalline hydroxyapatites synthesized by mechanical alloying. , 2019, , 81-117.		1
43	Stabilization of ZrO2 matrix: Revisiting the â€~archaic' issue with a peculiar example. Scripta Materialia, 2019, 162, 408-411.	5.2	1
44	Dielectric relaxation, AC conductivity behavior and its relation to microstructure in mechanochemically synthesized Mn-doped CeO2 nanocrystals. Solid State Sciences, 2019, 87, 93-100.	3.2	11
45	Evaluating the efficiency of grain boundary serrations in attenuating high-temperature hot corrosion degradation in Alloy 617. Corrosion Science, 2019, 149, 164-177.	6.6	17
46	Microstructure, optical and electrical characterizations of nanocrystalline ZnAl2O4 spinel synthesized by mechanical alloying: Effect of sintering on microstructure and properties. Physica E: Low-Dimensional Systems and Nanostructures, 2019, 108, 411-420.	2.7	27
47	Microstructure and Electrical Characterization of Thermoelectric Nanocrystalline Bi2 Te3 Synthesized by Mechanical Alloying. Materials Research, 2019, 22, .	1.3	7
48	Size Tunable Cesium Antimony Chloride Perovskite Nanowires and Nanorods. Chemistry of Materials, 2018, 30, 2135-2142.	6.7	132
49	Microstructure, optical, dielectric and electrical characterizations of Mn doped ZnO nanocrystals synthesized by mechanical alloying. Ceramics International, 2018, 44, 7110-7121.	4.8	32
50	Structural and magnetic properties of La2Ni1â^'Co MnO6 compounds. Materials Research Bulletin, 2018, 102, 248-256.	5.2	16
51	A critical evaluation on efficacy of recrystallization vs. strain induced boundary migration in achieving grain boundary engineered microstructure in a Ni-base superalloy. Acta Materialia, 2018, 146, 187-201.	7.9	120
52	One step synthesized In2O3 alloyed CeO2 nanoparticles: Microstructure, phase stability investigation and charge transport properties. Journal of Alloys and Compounds, 2018, 749, 724-733.	5.5	3
53	Microstructure, optical and electrical characterizations of Mn doped ZnS nanocrystals synthesized by mechanical alloying. Materials Research Bulletin, 2018, 97, 169-175.	5.2	28
54	Microstructure evolution during low-strain thermo-mechanical processing and its repercussion on intergranular corrosion in alloy 600H. Materials Characterization, 2018, 145, 582-593.	4.4	26

#	Article	IF	CITATIONS
55	Mechanosynthesis of Nanocrystalline Fully Stabilized bcc γ-phase of Bi2O3 without Any Additive: Manifestation of Ferroelasticity in Microstructure, Optical, and Transport Properties. Crystal Growth and Design, 2018, 18, 6564-6572.	3.0	18
56	Exploring (bio)catalytic activities of structurally characterised Cu( <scp>ii</scp> ) and Mn( <scp>iii</scp> ) complexes: histidine recognition and photocatalytic application of Cu( <scp>ii</scp> ) complex and derived CuO nano-cubes. Dalton Transactions, 2018, 47, 14008-14016.	3.3	6
57	Individual and synergistic influences of microstructural features on intergranular corrosion behavior in extra-low carbon type 304L austenitic stainless steel. Corrosion Science, 2018, 139, 319-332.	6.6	45
58	Microstructure characterization of intermetallic (Ni-Ti)3C nanocarbide compound synthesized by mechanical alloying of elemental powders. Ceramics International, 2018, 44, 14857-14864.	4.8	1
59	Hydrothermal synthesis of polyaniline intercalated vanadium oxide xerogel hybrid nanocomposites: effective control of morphology and structural characterization. New Journal of Chemistry, 2017, 41, 3634-3645.	2.8	50
60	Microstructure and electrical transport phenomenon of yttria alloyed nanocrystalline ceria solid solution synthesized by mechanical alloying. Materials Research Bulletin, 2017, 93, 333-341.	5.2	6
61	Alteration of magnetic behavior and microstructural distortion of EuMnO3 by partial substitution of Eu with monovalent Na. Journal of Alloys and Compounds, 2017, 715, 214-223.	5.5	2
62	Microstructure characterization of hydrothermally synthesized PANI/V2O5·nH2O heterojunction photocatalyst for visible light induced photodegradation of organic pollutants and non-absorbing colorless molecules. Journal of Hazardous Materials, 2017, 339, 161-173.	12.4	88
63	Influence of processing parameters on dynamic recrystallization and the associated annealing twin boundary evolution in a nickel base superalloy. Materials Science & Engineering A: Structural Materials: Properties, Microstructure and Processing, 2017, 700, 49-58.	5.6	103
64	Electrical transport and dielectric modulus formalism of CuO doped ZrO 2 partially stabilized solid solution. Materials Research Bulletin, 2017, 88, 272-280.	5.2	10
65	Targeting low-cost type-II heterostructures: Synthesis, structure and photoreactivity. Journal of Alloys and Compounds, 2017, 698, 944-956.	5.5	20
66	Microstructure correlated electrical conductivity of Manganese alloyed nanocrystalline cubic zirconia synthesized by mechanical alloying. Advanced Powder Technology, 2017, 28, 618-628.	4.1	8
67	Through-thickness microstructural evolution during grain boundary engineering type thermomechanical processing and its implication on sensitization behavior in austenitic stainless steel. Materials Characterization, 2017, 134, 134-142.	4.4	22
68	Effect of doping (Mg,Mn,Zn) on the microstructure and mechanical properties of spark plasma sintered hydroxyapatites synthesized by mechanical alloying. Ceramics International, 2017, 43, 2389-2397.	4.8	51
69	Structural Characterization and Electrical Conductivity of Mechanically Alloyed 10mol% In2O3–Doped CeO2 Nanoparticles. Current Physical Chemistry, 2017, 7, .	0.2	1
70	Effect of Material Behavior on Dynamic Characteristics Determination of Marine Propeller Blade Using Finite Element Analysis. Procedia Engineering, 2016, 144, 767-774.	1.2	3
71	Sintering behavior and growth mechanism of β-TCP in nanocrystalline hydroxyapatite synthesized by mechanical alloying. Ceramics International, 2016, 42, 13176-13182.	4.8	14
72	Microstructure and optical characterizations of mechanosynthesized nanocrystalline semiconducting ZrTiO4 compound. Journal of Physics and Chemistry of Solids, 2016, 95, 56-64.	4.0	7

#	Article	IF	CITATIONS
73	Structural, Optical Characterization and Growth Mechanism of Kadamba Flower like ZnO Nanocrystals Synthesized by a Simple Chemical Route ChemistrySelect, 2016, 1, 3705-3712.	1.5	7
74	Room temperature mechanosynthesis and microstructure characterization of nanocrystalline Si0.9Al0.1C. Materials Chemistry and Physics, 2016, 169, 186-191.	4.0	3
75	Structure, optical and magnetic characterizations of Mn doped ZnS dilute magnetic semiconductor synthesized by mechanical alloying. Advanced Powder Technology, 2016, 27, 1790-1799.	4.1	7
76	Microstructure characterization and electrical transport of nanocrystalline Zn0.90Mn0.100 semiconductors synthesized by mechanical alloying. Materials Research Bulletin, 2016, 77, 138-146.	5.2	5
77	Facile synthesis of SnO <sub>2</sub> –PbS nanocomposites with controlled structure for applications in photocatalysis. Nanoscale, 2016, 8, 2727-2739.	5.6	60
78	Effect of sodium doping on the microstructure, lattice distortion and magnetic properties of GdMnO <sub>3</sub> tiny single crystals. RSC Advances, 2016, 6, 20609-20620.	3.6	37
79	Investigation of dielectric and electrical behaviour of nanocrystalline Zn1â^'Mn O (x=0 to 0.10) semiconductors synthesized by mechanical alloying. Physica E: Low-Dimensional Systems and Nanostructures, 2016, 81, 122-130.	2.7	5
80	Magnesium substitution in carbonated hydroxyapatite: Structural and microstructural characterization by Rietveld's refinement. Materials Chemistry and Physics, 2016, 170, 319-329.	4.0	51
81	Structure and microstructure dependent ionic conductivity in 10 mol% Dy2O3 doped CeO2 nanoparticles synthesized by mechanical alloying. Materials Research Bulletin, 2016, 73, 446-451.	5.2	9
82	Photoswitching and Thermoresponsive Properties of Conjugated Multiâ€chromophore Nanostructured Materials. Small, 2015, 11, 6317-6324.	10.0	13
83	Effect of Manganese (II) Oxide on microstructure and ionic transport properties of nanostructured cubic zirconia. Electrochimica Acta, 2015, 170, 360-368.	5.2	16
84	Mechanical preparation of nanocrystalline biocompatible single-phase Mn-doped A-type carbonated hydroxyapatite (A-cHAp): effect of Mn doping on microstructure. Dalton Transactions, 2015, 44, 20087-20097.	3.3	24
85	One step ultrafast mechanosynthesis of nanocrystalline cubic Ti0.9Al0.1B and its microstructure evolution. Physica E: Low-Dimensional Systems and Nanostructures, 2015, 68, 93-101.	2.7	2
86	Structural interpretation of chemically synthesized ZnO nanorod and its application in lithium ion battery. Applied Surface Science, 2015, 329, 206-211.	6.1	30
87	Structural interpretation, growth mechanism and optical properties of ZnO nanorods synthesized by a simple wet chemical route. RSC Advances, 2015, 5, 23101-23113.	3.6	52
88	Influence of Size and Shape on the Photocatalytic Properties of SnO <sub>2</sub> Nanocrystals. ChemPhysChem, 2015, 16, 1017-1025.	2.1	64
89	Structural and microstructural interpretations of Zn-doped biocompatible bone-like carbonated hydroxyapatite synthesized by mechanical alloying. Journal of Applied Crystallography, 2015, 48, 138-148.	4.5	14
90	Microstructure characterization and electrical transport properties of nanocrystalline Fe and Fe-doped cubic zirconia cermets synthesized by mechanical alloying. Materials Research Bulletin, 2015, 68, 66-74.	5.2	11

#	Article	IF	CITATIONS
91	Effects of monovalent cation doping on the structure, microstructure, lattice distortion and magnetic behavior of single crystalline NdMnO <sub>3</sub> compounds. Dalton Transactions, 2015, 44, 17229-17240.	3.3	31
92	Electric modulus formalism and electrical transport property of ball mill synthesized nanocrystalline Mn doped ZrO2 solid solution. Physica B: Condensed Matter, 2015, 479, 67-73.	2.7	8
93	Electrical transport properties of nanocrystalline nonstoichiometric nickel ferrite at and above room temperature. Physica B: Condensed Matter, 2015, 457, 225-231.	2.7	7
94	Microstructure characterization and electrical transport of nanocrystalline CdZnS quantum dots. Physica E: Low-Dimensional Systems and Nanostructures, 2015, 66, 59-66.	2.7	9
95	Anomalous electrical transport mechanism in ternary carbide Ti0.9Al0.1C above room temperature. Physica B: Condensed Matter, 2014, 447, 1-6.	2.7	4
96	Structural and magnetic characterizations of undoped and K-doped NdMnO3 single crystals synthesized by sol–gel route: A comparative study. Powder Technology, 2014, 254, 538-547.	4.2	16
97	Structural interpretation of SnO <sub>2</sub> nanocrystals of different morphologies synthesized by microwave irradiation and hydrothermal methods. CrystEngComm, 2014, 16, 1079-1090.	2.6	57
98	Microstructure and photoluminescence properties of ternary Cd0.2Zn0.8S quantum dots synthesized by mechanical alloying. Journal of Nanoparticle Research, 2014, 16, 1.	1.9	9
99	Activation behavior and dielectric relaxation of nanocrystalline zinc ferrite. Materials Research Bulletin, 2014, 60, 446-452.	5.2	7
100	Biocompatible nanocrystalline natural bonelike carbonated hydroxyapatite synthesized by mechanical alloying in a record minimum time. Materials Science and Engineering C, 2014, 42, 647-656.	7.3	44
101	Ultrafast one step mechanosynthesis of nanocrystalline cubic Ti0.9Si0.1B and its microstructure characterization. Powder Technology, 2014, 264, 265-272.	4.2	0
102	Microstructure and optical characterizations of mechanosynthesized nanocrystalline (Ti0.9Si0.1)N. Powder Technology, 2013, 241, 28-35.	4.2	0
103	Microstructural evolution of nanostructured Ti0.7Ni0.3N prepared by reactive ball-milling. Materials Research Bulletin, 2013, 48, 3129-3135.	5.2	5
104	Microstructure and positron annihilation studies of mechanosynthesized CdFe <sub>2</sub> O <sub>4</sub> . Journal of Asian Ceramic Societies, 2013, 1, 356-361.	2.3	5
105	Microstructure characterization and electrical transport of nanocrystalline ZrO2–CeO2 solid solution. Materials Research Bulletin, 2013, 48, 3892-3900.	5.2	5
106	XRD and HRTEM characterization of mechanosynthesized Ti0.9W0.1C cermet. Journal of Alloys and Compounds, 2013, 581, 710-716.	5.5	8
107	One step quickest mechanosynthesis of nanocrystalline Ti0.9Si0.1C and its microstructure characterization. Journal of Alloys and Compounds, 2013, 557, 47-52.	5.5	4
108	Structural and microstructural characterizations of nanocrystalline hydroxyapatite synthesized by mechanical alloying. Materials Science and Engineering C, 2013, 33, 2891-2898.	7.3	24

#	Article	IF	CITATIONS
109	Microstructural, magnetic and optical characterizations of nanocrystalline Zn1â^'xMnxO dilute magnetic semiconductors synthesized by mechanical alloying. Journal of Alloys and Compounds, 2012, 519, 112-122.	5.5	16
110	Microstructural changes and effect of variation of lattice strain on positron annihilation lifetime parameters of zinc ferrite nanocomposites prepared by high enegy ball-milling. Materials Research, 2012, 15, 1022-1028.	1.3	16
111	Microstructural, optical and quantum confinement effect study of mechanically synthesized ZnTe quantum dots. Acta Materialia, 2012, 60, 131-138.	7.9	22
112	One-step mechanosynthesis of nano structured Ti(CxN1â°'x) cermets at room temperature and their microstructure characterization. Materials Chemistry and Physics, 2012, 134, 1088-1096.	4.0	5
113	Quickest ever single-step mechanosynthesis of Cd0.5Zn0.5S quantum dots: Nanostructure and optical characterizations. Materials Research Bulletin, 2012, 47, 1062-1072.	5.2	37
114	Mechanosynthesis of nanocrystalline Ti0.9C0.1N at room temperature and its microstructural aspects. Materials Science & Engineering A: Structural Materials: Properties, Microstructure and Processing, 2012, 534, 400-407.	5.6	10
115	Microstructural evolution of nanostructured Ti0.9Al0.1N prepared by reactive ball-milling. Journal of Alloys and Compounds, 2011, 509, 620-626.	5.5	8
116	Mechanochemical solid state synthesis of (Cd0.8Zn0.2)S quantum dots: Microstructure and optical characterizations. Journal of Alloys and Compounds, 2011, 509, 4176-4184.	5.5	29
117	Quickest single-step one pot mechanosynthesis and characterization of ZnTe quantum dots. Journal of Alloys and Compounds, 2011, 509, 5567-5570.	5.5	8
118	Quickest Single-Step Mechanosynthesis of CdS Quantum Dots and Their Microstructure Characterization. Journal of Nanoscience and Nanotechnology, 2011, 11, 4771-4780.	0.9	12
119	Preparation of nanodimensional CdS by chemical dipping technique and their characterization. Materials Research, 2011, 14, 17-20.	1.3	27
120	Anomalous electrical transport properties of nonstoichiometric nickel ferrite below room temperature. Materials Research Bulletin, 2011, 46, 1055-1064.	5.2	11
121	One-step fastest method of nanocrystalline CuAlS2 chalcopyrite synthesis, and its nanostructure characterization. Journal of Nanoparticle Research, 2011, 13, 2343-2350.	1.9	9
122	Dielectric relaxation and magnetic field dependent alternating current conductivity of nanocrystalline cadmium–zinc ferrite below room temperature. Physica B: Condensed Matter, 2011, 406, 3261-3266.	2.7	14
123	Microstructure Characterization of Nanocrystalline Magnesium Ferrite Annealed at Elevated Temperatures by Rietvold Method JSRN Ceramics, 2011, 2011, 1-8 Microstructure, MAIssbauer, and Optical Characterizations of Nanocrystalline <mml:math< td=""><td>0.2</td><td>7</td></mml:math<>	0.2	7
124	xmlns:mml="http://www.w3.org/1998/Math/MathML"> <mml:mi mathvariant="bold"&gt;1±-<mml:math xmlns:mml="http://www.w3.org/1998/Math/MathML"&gt;<mml:msub><mml:mtext>Fe</mml:mtext><mml:mn mathvariant="bold"&gt;2</mml:mn </mml:msub><mml:msub><mml:mtext>O</mml:mtext><mml:mn< td=""><td>0.2</td><td>6</td></mml:mn<></mml:msub></mml:math </mml:mi 	0.2	6
125	mathvariant="bold">3 Synthesized by Chemical Route. ISRN Cerami Microstructure characterization of nanocrystalline TiC synthesized by mechanical alloying. Materials Chemistry and Physics, 2010, 120, 537-545.	4.0	57
126	Electrical transport behavior of nonstoichiometric magnesium–zinc ferrite. Materials Research Bulletin, 2010, 45, 954-960.	5.2	17

#	Article	IF	CITATIONS
127	Alternate current conductivity and dielectric properties of nonstoichiometric nanocrystalline Mg–Zn ferrite below room temperature. Physica E: Low-Dimensional Systems and Nanostructures, 2010, 42, 1397-1405.	2.7	8
128	In-situ high temperature annealing of nanostructured ZrTiO4 prepared by mechanical alloying. Physica E: Low-Dimensional Systems and Nanostructures, 2010, 42, 1772-1776.	2.7	2
129	Synthesis of nanocrystalline Cd–Zn ferrite by ball milling and its stability at elevated temperatures. Journal of Alloys and Compounds, 2010, 489, 91-98.	5.5	15
130	Mechanosynthesis of nanocrystalline titanium nitride and its microstructure characterization. Journal of Alloys and Compounds, 2010, 493, 192-196.	5.5	14
131	Preparation of ternary Ti0.9Ni0.1C cermets by mechanical alloying: Microstructure characterization by Rietveld method and electron microscopy. Journal of Alloys and Compounds, 2010, 493, 666-671.	5.5	18
132	Microstructure characterization of ball-mill prepared ternary Ti0.9Al0.1C by X-ray diffraction and electron microscopy. Journal of Alloys and Compounds, 2010, 501, 198-203.	5.5	15
133	Microstructure characterization of nanocrystalline Fe3C synthesized by high-energy ball milling. Journal of Alloys and Compounds, 2009, 477, 127-132.	5.5	44
134	Microstructure characterization of nanocrystalline Ni3C synthesized by high-energy ball milling. Journal of Alloys and Compounds, 2009, 479, 193-200.	5.5	58
135	Microstructural characterization of nanocrystalline SiC synthesized by high-energy ball-milling. Journal of Alloys and Compounds, 2009, 486, 480-485.	5.5	41
136	Electrical transport properties of nanocrystalline zinc ferrite. Physica E: Low-Dimensional Systems and Nanostructures, 2008, 40, 2686-2693.	2.7	8
137	Phase Stability of Nanocrystalline Mg–Zn Ferrite at Elevated Temperatures. Japanese Journal of Applied Physics, 2008, 47, 8667-8672.	1.5	20
138	PbZr1â^xTixO3by soft synthesis: Structural aspects. Physical Review B, 2007, 76, .	3.2	7
139	Atomic-Scale Structure of Nanosized Titania and Titanate: Particles, Wires, and Tubes. Chemistry of Materials, 2007, 19, 6180-6186.	6.7	60
140	Microstructure characterization and polymorphic transformation kinetic study of ball-milled nanocrystalline a-TiO2–20mol% m-ZrO2 mixture by X-ray diffraction and electron microscopy. Physica E: Low-Dimensional Systems and Nanostructures, 2007, 36, 17-27.	2.7	10
141	Microstructure characterization of mechanosynthesized nanocrystalline NiFe2O4 by Rietveld's analysis. Physica E: Low-Dimensional Systems and Nanostructures, 2007, 39, 175-184.	2.7	55
142	Microstructure characterization and phase transformation kinetics of ball-mill prepared nanocrystalline Mg–Zn-ferrite by Rietveld's analysis and electron microscopy. Materials Chemistry and Physics, 2007, 105, 31-37.	4.0	29
143	Annealing effect on nano-ZnO powder studied from positron lifetime and optical absorption spectroscopy. Journal of Applied Physics, 2006, 100, 114328.	2.5	135
144	X-ray characterization and phase transformation kinetics of ball-mill prepared nanocrystalline Mg–Zn-ferrite at elevated temperatures. Physica E: Low-Dimensional Systems and Nanostructures, 2006, 33, 367-369.	2.7	10

#	Article	IF	CITATIONS
145	Preparation of nanocrystalline microwave dielectric Zn2TiO4 and ZnTiO3 mixture and X-ray microstructure characterization by Rietveld method. Physica E: Low-Dimensional Systems and Nanostructures, 2006, 33, 69-76.	2.7	49
146	Preparation of nanocrystalline CuAlFeS2-mixed chalcopyrite by high-energy ball milling. Physica E: Low-Dimensional Systems and Nanostructures, 2006, 33, 66-68.	2.7	5
147	Order–disorder transition in nanocrystalline Ni3Al prepared by a chemical route. Physica E: Low-Dimensional Systems and Nanostructures, 2006, 31, 224-227.	2.7	2
148	Mechanosynthesis of nanocrystalline chalcopyrite. Physica E: Low-Dimensional Systems and Nanostructures, 2006, 33, 144-146.	2.7	18
149	Microstructure characterization of ball-mill-prepared nanocrystalline CaCu3Ti4O12 by Rietveld method. Physica E: Low-Dimensional Systems and Nanostructures, 2006, 33, 160-168.	2.7	14
150	Nanocrystalline CaTiO3 prepared by soft-chemical route. Physica E: Low-Dimensional Systems and Nanostructures, 2005, 25, 421-424.	2.7	10
151	Microstructure characterization and phase transformation kinetic study of ball-milled m-ZrO2–30mol% a-TiO2 mixture by Rietveld method. Physica E: Low-Dimensional Systems and Nanostructures, 2005, 27, 405-419.	2.7	4
152	X-ray characterization and phase transformation kinetics of ball-mill prepared nanocrystalline Mg–Ni-ferrite at elevated temperatures. Physica E: Low-Dimensional Systems and Nanostructures, 2005, 28, 43-49.	2.7	12
153	Microstructure characterization and cation distribution of nanocrystalline magnesium ferrite prepared by ball milling. Materials Chemistry and Physics, 2005, 93, 224-230.	4.0	182
154	Electrical conductivity in nanostructured magnetite–hematite composites produced by mechanical milling. Journal of Magnetism and Magnetic Materials, 2005, 288, 301-306.	2.3	17
155	X-ray microstructure characterization of ball-milled nanocrystalline microwave dielectric CaZrO3by Rietveld method. Journal of Applied Crystallography, 2005, 38, 291-298.	4.5	31
156	Structure of nanocrystalline MgFe2O4from X-ray diffraction, Rietveld and atomic pair distribution function analysis. Journal of Applied Crystallography, 2005, 38, 772-779.	4.5	91
157	Microstructure characterization of nanocrystalline ZrSiO4synthesized by ball-milling and high-temperature annealing. Journal of Applied Crystallography, 2005, 38, 951-957.	4.5	23
158	Study of Microstructural Defect Parameters in Vanadium–Aluminium Alloys using Warren–Averbach Method and Modified Rietveld Technique. Japanese Journal of Applied Physics, 2005, 44, 6678-6682.	1.5	3
159	Microstructure Characterization and Phase Transformation Kinetic Study of Mechanosynthesized Non-Stoichiometric CdFe2O4by Rietveld's Analysis. Japanese Journal of Applied Physics, 2004, 43, 5455-5464.	1.5	16
160	Characterization of crystalline structure of ball-milled nano-Ni–Zn-ferrite by Rietveld method. Materials Chemistry and Physics, 2004, 84, 291-301.	4.0	81
161	Microstructure characterization of ball milled prepared nanocrystalline perovskite CaTiO3 by Rietveld method. Materials Chemistry and Physics, 2004, 86, 284-292.	4.0	35
162	Synthesis of nanocomposites comprising iron and barium hexaferrites. Journal of Magnetism and Magnetic Materials, 2004, 269, 42-47.	2.3	32

#	Article	IF	CITATIONS
163	Characterization of crystalline structure of ball-milled nano-Ni–Zn-ferrite by Rietveld method. Materials Chemistry and Physics, 2004, 84, 291-291.	4.0	5
164	X-ray diffraction studies of the decomposition and microstructural characterization of cold-worked powders of Cu–15Ni–Sn alloys by Rietveld analysis. Journal of Alloys and Compounds, 2004, 377, 103-116.	5.5	40
165	Microstructure characterization and phase transformation kinetics of ball-milled prepared nanocrystalline Zn2TiO4 by Rietveld method. Materials Chemistry and Physics, 2003, 82, 837-847.	4.0	49
166	Microstructure characterization and phase transformation kinetics of polymorphic transformed ball milled a-TiO2–10 mol% m-ZrO2 mixture by Rietveld method. Materials Chemistry and Physics, 2003, 82, 848-859.	4.0	35
167	Microstructure characterization of polymorphic transformed ball-milled anatase TiO2 by Rietveld method. Materials Chemistry and Physics, 2003, 77, 153-164.	4.0	67
168	Microstructure characterization of high energy ball-milled nanocrystalline V2O5 by Rietveld analysis. Materials Chemistry and Physics, 2003, 77, 868-877.	4.0	26
169	Rietveld analysis of polymorphic transformations of ball milled anatase TiO2. Materials Chemistry and Physics, 2003, 80, 73-81.	4.0	44
170	Preparation of zinc ferrite by high-energy ball-milling and microstructure characterization by Rietveld's analysis. Materials Chemistry and Physics, 2003, 82, 27-37.	4.0	160
171	Preparation and microstructure characterization of m-ZrO2–20 mol% a-TiO2 ball milled mixture by Rietveld method. Materials Science & Engineering A: Structural Materials: Properties, Microstructure and Processing, 2003, 359, 269-279.	5.6	6
172	Phase transformation kinetic study and microstructure characterization of ball-milledm-ZrO2–10â€mol%a-TiO2by Rietveld method. Journal of Applied Crystallography, 2003, 36, 260-268.	4.5	31
173	X-ray characterization of nanocrystalline Ni3Fe. Journal of Alloys and Compounds, 2002, 343, 192-198.	5.5	17
174	Microstructural evolution on ball-milling elemental blends of Ni, Al and Ti by Rietveld's method. Materials Chemistry and Physics, 2002, 74, 167-176.	4.0	22
175	Preparation and microstructure characterization of ball-milled ZrO2powder by the Rietveld method: monoclinic to cubic phase transformation without any additive. Journal of Applied Crystallography, 2002, 35, 517-525.	4.5	91
176	Nanophase iron oxides by ball-mill grinding and their Mössbauer characterization. Journal of Alloys and Compounds, 2001, 326, 292-297.	5.5	33
177	X-ray studies on the kinetics of microstructural evolution of Ni3Al synthesized by ball milling elemental powders. Materials Chemistry and Physics, 2001, 68, 166-174.	4.0	32
178	Effect of alloying on the microstructure and mechanical properties of Ni3Al. Journal of Alloys and Compounds, 1998, 265, 249-256.	5.5	26
179	Characterisation of Deformed and As-cast Microstructure of Copper-Aluminium-Iron Alloys-II: Influence of Increased Fe Solute (α+β-Phase). Japanese Journal of Applied Physics, 1996, 35, 1836-1841.	1.5	5
180	Microstructure and Mechanical Property of α-Al–Zn–Cu Alloys Aged at Room Temperature. Materials Transactions, JIM, 1995, 36, 490-495.	0.9	13

#	Article	IF	CITATIONS
181	Microstructure and Phase-Transformation Studies of Cu-Ni-Sn Alloys. Japanese Journal of Applied Physics, 1995, 34, 1619-1626.	1.5	14
182	X-ray powder profile analyses on nanostructured niobium metal powders. Scripta Materialia, 1995, 5, 53-61.	0.5	21
183	Low temperature mullite formation from sol-gel precursors by hot pressing. Journal of Materials Research, 1994, 9, 2474-2475.	2.6	2
184	Stability of cubic phase in nanocrystalline ZrO <sub>2</sub> . Journal of Materials Research, 1994, 9, 263-265.	2.6	75
185	Microstructural Characterisation of Hexagonal(Ag,Cu)Zn4Alloys in the Deformed and As-Cast State. Japanese Journal of Applied Physics, 1994, 33, 1443-1449.	1.5	4
186	Synthesis of aluminium matrix composites containing nanocrystalline oxide phases. Bulletin of Materials Science, 1994, 17, 849-853.	1.7	6
187	Structural characterization of the CuIn intermetallic phase produced by interfacial reactions in Cu/In bimetallic films. Thin Solid Films, 1993, 229, 140-142.	1.8	12
188	Synthesis of nanocrystalline nickel-zinc ferrite by the sol-gel method. Journal of Magnetism and Magnetic Materials, 1993, 127, 214-218.	2.3	151
189	Characterization of Deformed and As-cast Microstructure of Copper-Aluminium-Iron Alloys (α-Phase). Japanese Journal of Applied Physics, 1993, 32, 1164-1170.	1.5	10
190	An xâ€ray diffraction line profile analysis on the microstructure of coldâ€worked faceâ€centeredâ€cubic Cuâ€Mnâ€5i alloys: Effects of Mn and Si as solutes. Journal of Applied Physics, 1988, 64, 2324-2327.	2.5	11
191	An xâ€ray diffraction study of lattice imperfections in coldâ€worked faceâ€centeredâ€cubic alloys. VI. Copperâ€aluminum (α phase). Journal of Applied Physics, 1987, 62, 1521-1523.	2.5	21